Simultaneous Wireless Electrophysiological and Neurochemical Monitoring

Kartikeya Murari[a], Mohsen Mollazadeh[a], Nitish Thakor[a] and Gert Cauwenberghs[b]

[a]Department of Biomedical Engineering, Johns Hopkins University School of Medicine, Baltimore, MD, USA;
[b]Division of Biology, University of California at San Diego, La Jolla, CA, USA

ABSTRACT

Information processing and propagation in the central nervous system is mostly electrical in nature. At synapses, the insulating gaps between neurons, electrical signals cause the release of chemical messengers called neurotransmitters which travel across the synapse and modulate the postsynaptic neuron electrical activity. The interrelated nature of these signals and their implication in several clinical and basic neural pathways motivate their simultaneous monitoring. We present an integrated system for continuous acquisition of both data modalities in awake behaving rats. It features one channel each of a configurable electrophysiological and a neurochemical acquisition system. The electrophysiological system comprises of a 40 dB gain fully differential amplifier with tunable bandwidth from 140 to 8200 Hz. The amplifier offers noise below 2 μV_{rms} for all bandwidth settings. The neurochemical module features a picoampere sensitivity potentiostat with a dynamic range spanning 6 decades from picoamperes to micoamperes. Both systems have independent on-chip configurable $\Delta\Sigma$ ADCs with programmable digital gain and resolution. The system was also interfaced to a wireless power harvesting and telemetry module capable of powering up the circuits, providing clock for ADC operation and telemeter out the data at up to 32 kbps over 4 cm with a bit error rate (BER) $< 10^{-5}$. Characterization and experimental results from both the electrophysiological and neurochemical modules as well as the full system are presented.

Keywords: Electrophysiology, neural monitoring, neurochemistry, neurotransmitters, VLSI, biomedical implants, telemetry, inductive power harvesting

1. INTRODUCTION

Electrical and neurochemical activity are intricately related in the central nervous system. The presynaptic cells release excitatory or inhibitory neurotransmitters into the synapse[1] upon arrival of a nerve impulse. These chemical messenger molecules like dopamine, glutamate etc. bind to receptors on the postsynaptic cell and cause excitatory or inhibitory postsynaptic potentials (EPSPs and IPSPs). The neuron integrates all the postsynaptic potentials and decides whether to fire an action potential or not. The abnormal functioning of this signaling cascade causes severe damage to the underlying cellular substrates. In aging related neurodegenerative disorders like Parkinson's disease, the motor functions are disrupted due to the death of dopaminergic neurons in substantia niagra which project to the striatum. This pathway is shown in Fig. 1. In case of cardiac arrest, uncontrolled neurotransmitter release due to the absence of modulatory electrical activity in the brain is the basis of glutamate excitotoxicity which leads to excessive neuronal cell death. The interplay between electrical and neurochemical activity is also implicated in several basic neural pathways like rewards and learning.

Several methods have been reported in the literature for monitoring neurotransmitters activity. Some of these are optical and chromatographic methods, positron emission tomography (PET) and single photon emission computerized tomography (SPECT).[2–4] These methods are mostly indirect, detecting products of reactions involving the neurotransmitter, rather than the neurotransmitter itself. Alternatively, electrochemical detection is a direct analytical method that can be applied to a subset of neurotransmitters that are electrochemically active.[5] The technique utilizes an oxidation/reduction reaction involving the neurochemical that generates a current proportional to the concentration of the species. While several electrochemical analyses exist to quantify redox reactions, including amperometry, cyclic voltametry, chronocoulometry etc.,[6] we will restrict ourselves to chronoamperometry where the current is monitored over time as a measure of concentration..
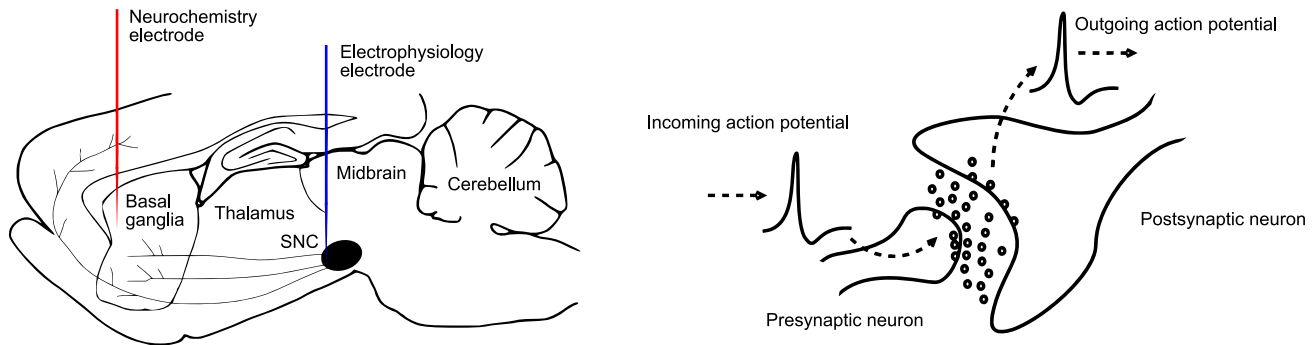
Figure 1. Neurochemical and neuropotential signalling is related in the nervous system. *Left:* the pathway implicated in Parkinson's disease where dopaminergic neurons in the substantia nigra pars compacta (SNC) die. Electrodes show a potential use of simultaneous neurochemical and neuropotential monitoring. *Right:* details of how the electrical and chemical signalling is related.

While synapses transfer information locally in insulating gaps through neurochemical signaling, signals are transmitted over a longer range in the form of electrical action potentials traveling across the central nervous system.[1] The electrical activity of the brain can be recorded from within the brain (spike or local field potentials), the surface of the brain (electrocorticogram or ECoG), or from the scalp (electroencephalogram or EEG). These signals encode information about the underlying brain function which potentially can be extracted by signal processing methods. Recently, neural recordings have also been used as a channel to communicate with the brain. These Brain Computer Interfaces help locked-in patients communicate with the outside world.[7-9] Another common application area is the recording of electrocorticograms in clinical investigations of neurological disorders such as epilepsy. However, due to the large-scale instrumentation needed to implement EEG recording systems, these systems are mostly restricted to hospitals. In all these applications, miniaturized recording systems are required so that they can be integrated into the daily lives for those who need it.

Here, we present an integrated neural interface system for the simultaneous acquisition of neuropotential and neurochemical activity from the brain. The neurochemical module consists of a wide-range, picoampere sensitivity potentiostat for the electrochemical detection of neurotransmitters concentration down to nanomolar range while consuming 5 μW of power. The electrophysiological module consists of a 40 dB gain amplifier with a tunable bandpass bandwidth up to 8.2 kHz in order to isolate the signal of interest - spikes, LFPs, ECoG or EEG. The amplifier consumes 40 μW of power for the full bandwidth. Both modules have incremental $\Delta\Sigma$ analog-to-digital converters which allow programmable digital gain and measurement resolution based on the dynamic range of the acquired signal. The total digital power consumption was 100 μW. The difference in the spectral content of electrical (Hz to several hundred Hz) and neurochemical signals (mHz) is used to interleave the digitized bitstreams. The power harvesting and telemetry module uses electromagnetic induction at 4 MHz to power up the microchips, provide clocks and obtain data from them at up to 32 kbps at a distance of upto 4 cm with a bit error rate (BER) $< 10^{-5}$. In *in vitro* tests performed with the system, no significant interference was seen between the electrical recordings and potentiostatic recordings. Applications of the system to neuroscience include monitoring of EEG signals and glutamate concentration in rat somatosensory cortex following global ischemia.

2. SYSTEM DESCRIPTION

2.1 VLSI Potentiostat with Configurable Incremental $\Delta\Sigma$ ADC

Electrochemical analysis[5] is a fast, direct method of detecting and measuring the concentration of a subset of neurotransmitters that are electrochemically active like dopamine, nitric oxide etc. The principle of operation is that electroactive neurotransmitters get oxidized or reduced at electrode surfaces. For optimal reaction, the electrode must be at the redox potential of the reaction.[6] The reaction involves a transfer of electrons between the electrode and the species being detected which constitutes a current that is proportional to the concentration of the neurotransmitter, the electrode area and reaction kinetics parameters.
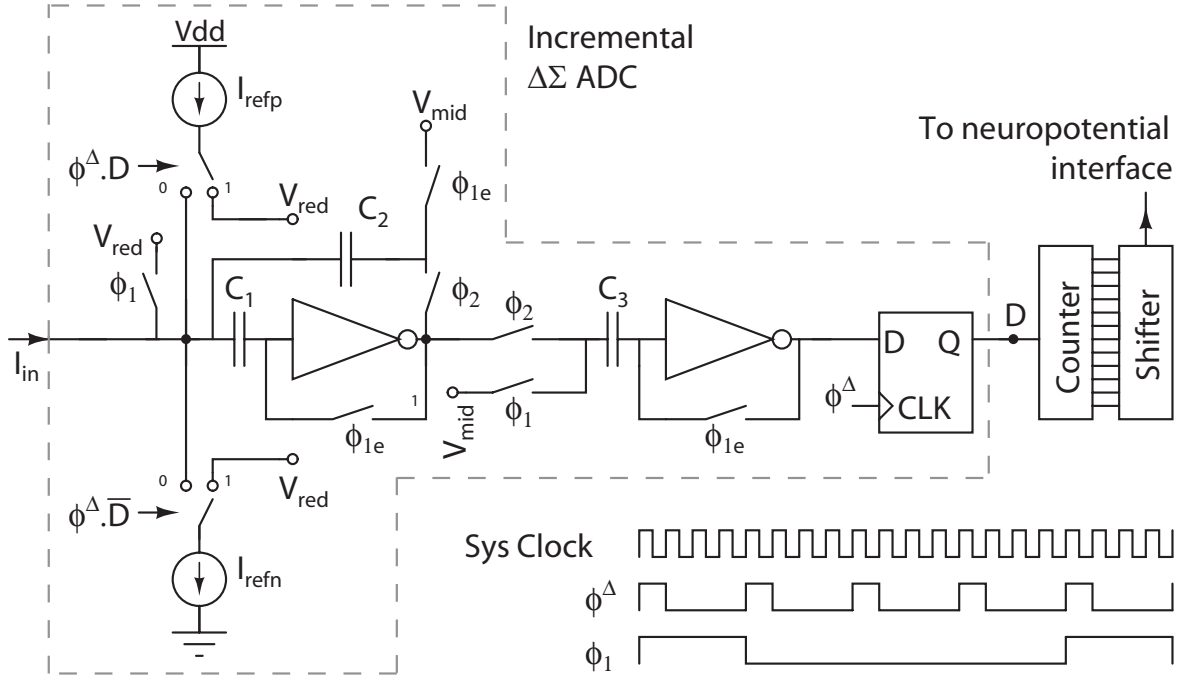
Figure 2. Schematic block diagram of the VLSI potentiostat circuitry. Clocks on the lower right show a toy example of gain 4 and oversampling ratio 4.

The instrumentation required for electrochemical sensing, a potentiostat, is a three terminal device[10] that maintains the aforementioned redox potential and simultaneously measures the redox current. With physiological concentrations of neurotransmitters, the currents involved are always below microamperes allowing a simplification to be made to the potentiostat. One of the three terminals is responsible for negating the effects of ohmic drops in solution. With the small currents being measured in our case, the potential drops are negligible, and a two terminal device can perform the required measurements.

Compared to commercial devices, integrated circuit technology offers low power, multiple channels, low noise, high sensitivity in a very small footprint. Over the years, several groups have presented VLSI potentiostat chips with one or multiple channels. Turner et al.[11] used a direct current-to-voltage conversion with an opamp and a resistor. In the work presented by Kakerow et al.,[12] the input current was integrated on a capacitor and the voltage across the capacitor was sampled as a measure of the current. Gore et al. described A semi-synchronous $\Delta\Sigma$ ADC based potentiostat.[13] We have previously designed a 16 channel potentiostat with configurable incremental $\Delta\Sigma$ analog to digital converter in our lab.[14] Mohseni et al. also used a programmable $\Delta\Sigma$ modulator along with a wireless interface in their design.[15]

Figure 2 shows the schematic diagram and operating clocks of the potentiostat circuitry. Non-overlapping clocks ϕ_1 and ϕ_2 are generated from ϕ^Δ. The ratio of periods of ϕ_1 and ϕ^Δ sets the oversampling ratio (resolution) of the ADC (4 in the example shown in Fig. 2, typically 2^8 to 2^{12}) . Rising edge of the clock ϕ_1 starts the conversion by charging the input capacitor C_1 to the redox potential V_{red}. Clock ϕ_{1e} occurs within ϕ_1 and resets the integration capacitor C_2 and the comparator capacitor C_3. The integration occurs during ϕ_2 and the integrated value is compared to the mid value V_{mid}. The comparator output is latched using ϕ^Δ. If the latched value D is high, a counter value is incremented and the $\Delta\Sigma$ reference current i_{refn} is subtracted from the input current until the comparator flips. Conversely, when D is low, the counter value does not change and the $\Delta\Sigma$ reference current i_{refp} is added to the input current until the comparator flips. Digital gain in the ADC is implemented by the duty cycle of the clock ϕ^Δ (4 in the example shown in Fig. 2). The gain is achieved by adding or subtracting the $\Delta\Sigma$ reference currents, i_{refp} and i_{refn}, to the input current I_{in} **only** during the high period of ϕ^Δ. The gain and OSR can can be prgrammed in the range 1-64 and 2^8-2^{12}. At the end of the integration period, before ϕ_1 goes high, the value in the counter is shifted into a parallel-in serial-out shift
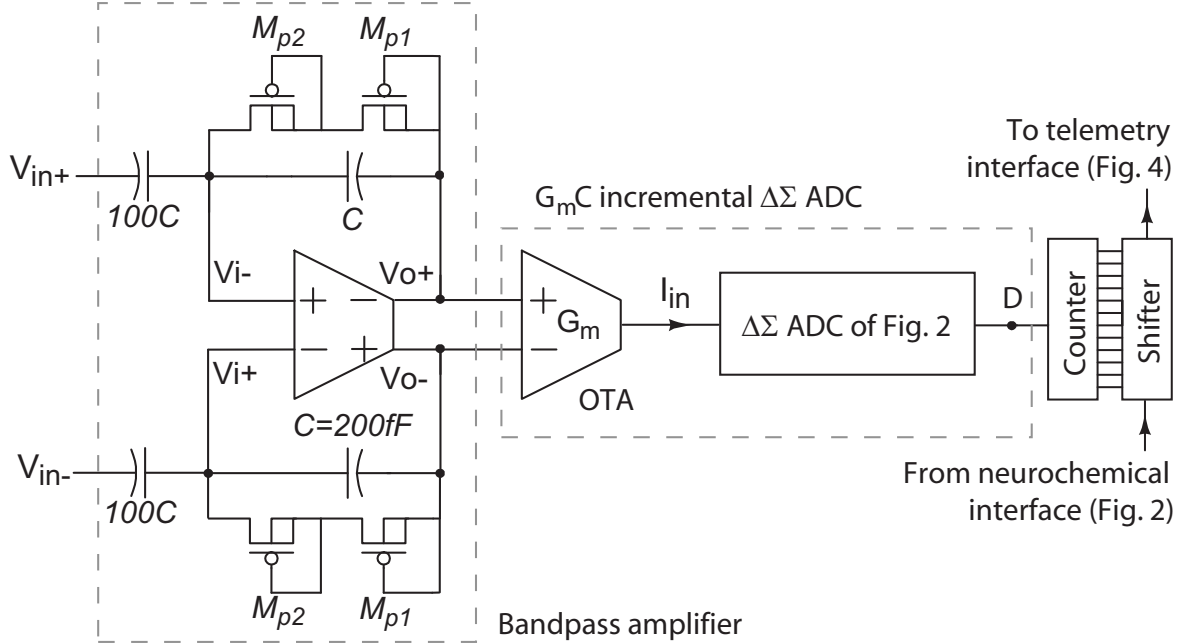
Figure 3. Functional block diagram for the neuropotential interface channel.

register and read out asynchronously.

2.2 Neuropotential Interface

Electrical activity in the brain originates as spikes from the firing of single neurons. This activity can be monitored if a small electrode is placed very close to the cell. As the electrode moves away from the source, it also picks up the current fields cause by the presynaptic and postsynaptic activity from other neurons. The resulting electrical activity can then be recorded as LFP, ECoG or EEG. These modalities of neural potentials occupy different frequency bands from 0.1 Hz to 5 kHz and have various amplitude range from 20 to 500 μV.[16] A versatile VLSI system which can interface to all these modalities is highly desirable. Several VLSI systems have been developed previously[17–31] to acquire different neural signals. Typically the range of frequencies covered by any one of these systems is limited to one or two signal modalities, to accommodate high efficiency for the targeted application.

We have designed a CMOS neural interface system with adjustable bandwidth, gain and ADC resolution. Figure 3 shows the block diagram of the neuropotential interface. The bandpass amplifier in the front-end offers fixed-gain (40 dB) amplification with tunable lowpass filtering from 140 Hz to 8.2 kHz. The midband gain is achieved by fixed ratio capacitors 100C/C. The dc component of the signal is removed using the highpass filter implemented using pseudo-resistor elements M_{p1} and M_{p2} and capacitor C (100 fF).[21] Two elements were used in series to increase the resistance and therefore decrease the highpass cutoff frequency. The bandpass amplifier was designed using a two stage fully differential amplifier with independent common mode feedback circuitry (CMFB) in each stage. The input transistors were chosen as p-channel devices to lower 1/f noise. They are also sized with large W/L to operate in the subthreshold region for the maximum bandwidth. The bias current of the amplifier is adjusted using a programmable DAC. A decrease in the bias current results in a decrease in the unity gain frequency and hence the bandwidth of the amplifier while maintaining the input transistors in the subthreshold region. The amplifier was designed for a phase margin of 62°.

The amplified neural signal is then digitized using a configurable incremental G_mC $\Delta\Sigma$ ADC. In order to digitize the differential output voltage of the amplifier, the amplified signals are first converted to a single ended current using a NMOS differential pair open transconductance amplifier (OTA) which also removes any remaining common mode signal. The OTA input transistors were sized long in order to increase the linear range of operation. The core of the ADC is same as the structure implemented in the potentiostat circuitry

and described in detail in the previous section. The ADC offers programmable resolution from 8 to 12 bits and digital gain of 1 to 4. The digitized output is then read out using a parallel-in serial-out shift register.

2.3 Wireless Power Delivery and Telemetry

In order to monitor both modalities of signals in awake behaving animals, the system needs to communicate with the outside word without any wires, i.e. both the power for the system operation and digitized data should be transmitted wirelessly to and from the system. Inductive coupling offers an attractive solution for transmitting power transcutaneously, since there is a range of RF frequencies (1-20 MHz) where tissue absorption is minimal.[32] A large sinusoidal voltage on the transmitter coil induces a voltage on the receiver coil which in turn is rectified and regulated to provide power. Previously, most VLSI monitoring systems have used separate links for power and data transmission due to high data bandwidth.[27, 33, 34] Since our system is fairly low bit rate, we have used the same inductive link for both data and power transfer.

Figure 4 shows the functional block diagram of the power harvesting and telemetry interface which was designed previously in our lab and implemented on a separate die.[35] We have chosen to work at 4 MHz frequency based on the power requirement and the system data rate. A class-E power amplifier on the transmitter side generates a large 4 MHz sine wave across a 2.5 cm radius coil. The induced magnetic field is picked up by the 1 cm radius receiver coil. The induced voltage is then rectified by a full-wave rectifier followed by a lowpass filter. The rectified signal is then regulated to provide a stable supply for system operation. There are two regulators in the interface system which provide two separate 3.3 V supply for digital and analog parts. Each can supply up to 2 mA of current. The clock extraction block also generates a 1 MHz clock for ADC operation of both channels. This removes the need for on chip oscillators as well as synchronizing both the neuropotential and neurochemical data.

The digitized sensor data in NRZ (non-return to zero) format is then transmitted over the same link via LSK (load-shift keying) modulation. This is accomplished by changing the resistance across the receiver coil which in turn changes the current in the transmitter coil. A coherent demodulator is implemented in the base station to extract the sensor data. Briefly, the received data is amplified (gain = 5), squared and low pass filtered (50 kHz) to extract the encoded information. The final output was then acquired using a DAQ card and read into a computer.

2.4 Neurochemical/Neuropotential Interface Strategy

While neurochemical and neuropotential signalling is tightly related in the nervous sytem, there are some crucial differences. As described in Sec. 1, electrical signals or action potentials travel down neurons to synapses. This
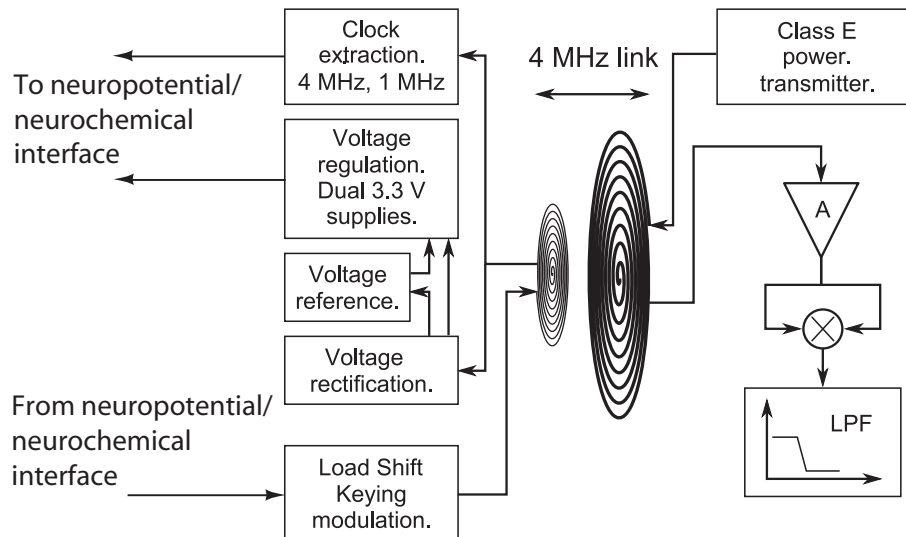

Figure 4. Functional block diagram for the power harvesting and telemetry block.

transfer is mediated by sequential opening and closing of ion channels that let in ions selelectively.[36] Typically an action potential lasts a few milliseconds thereby placing neuropotential activity in the several hundred hertz to kilohertz band. Depending on where the neuroptentials are measured from, electrical signals get low pass filtered and the spectrum of the information content can shift down to upto a few hundred hertz. Neurochemical activity, on the other hand, is mediated by chemicals that are released into the synapse. A neuron integrates all the electrical signals that it recieves and based on the result may release excitatory or inhibitory neurochemicals. These are then taken up by other cells and may cause downstream changes which activate ion channels leading to an action potential in the post-synaptic cell. As can be imagined, the processes involved in chemical signalling are slow. The changes occur on the order of hundreds of milliseconds to seconds. Thus the spectrum of neurochemical signals extends only up to a several hertz.

Our design[37] for the simultaneous monitoring of electrical and nueorchemical activity exploits the large difference in the frequency content of the signals. The ADCs for the neurochemical and the electrophysiological monitoring circuits can be programmed to sample in any arbitrary fashion. For example the potentiostat ADC may be set to sample at 5 Hz while the neuropotential ADC may be set to 1 kHz. Thus every 200 samples of the electrophysiological data will be interleaved with 1 sample of the neurochemical data. Since all the clocks are generated on chip using a single system clock which is supplied by the off-chip telemetry and power harvesting interface shown in Fig. 4, both the data streams are synchronized and can be read out serially by appropriately reading the output shift registers of Fig. 2 and Fig. 3. A simple state machine was implemented to carry out that task. Depending on the programming parameters, the state machine generates either 12 or 24 pulses on the clock used to read out the daisy-chained shift registers. Twelve pulses read out the neuropotential ADC value while 24 pulses read out both the neuropotential and the neurochemical ADCs.

3. RESULTS

The multimodal neural interface circuit was fabricated in a 0.5 μm 2 poly, 3 metal CMOS technology and occupies 1.5 mm$\times$1.5 mm of silicon area. The RF power harvesting and telemetry was fabricated in the same technology on a separate die and occupies 0.1 mm^2. Each block of the system was characterized individually and as a whole.

3.1 Potentiostat Characterization

Figure 5a shows the measured normalized digital output of the potentiostat for input currents swept in different ranges. A model 6430 sourcemeter (Kiethley Inc., Cleveland, OH) was programmed to vary the input current. The $\Delta\Sigma$ I_{ref} was set to 400 nA and the system clock was 1 MHz. The digital gain and OSR were programmed
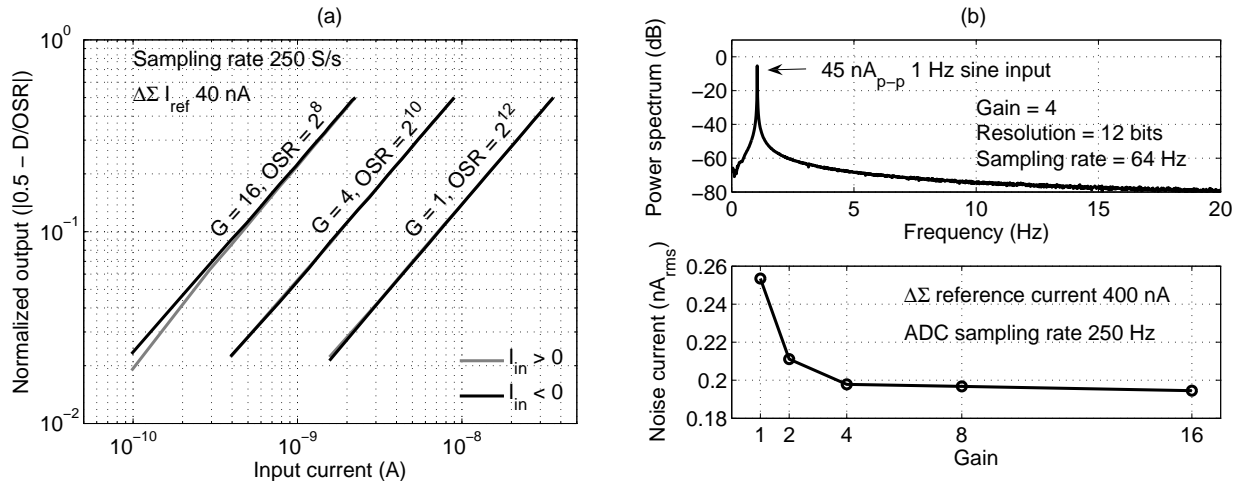

Figure 5. Characterization results from the potentiostat circuit. *Left:* Normalized digital output of the chip for several values of digital gain G, oversampling ratio OSR and both polarities of input currents. *Right top:* Power spectrum of the output corresponding to a 1 Hz 45 nA_{p-p} input current. *Right bottom:* Effect of gain on reducing input current noise.

individually for each setting for a sampling rate of 250 S/s. As it can be seen in the figure, the circuit offers a wide dynamic range for all gain and resolution settings.

Figure 5b shows the measured noise in the system. The top panel shows the power spectrum of the potentiostat output when presented with a 45 nA_{p-p} sinusoidal current at 1 Hz. The gain and OSR were set to 4 and 2^{12} respectively resulting in a sampling rate of 64 S/s. The bottom panel shows the effect of the programmed ADC gain on RMS current noise. The OSR was changed for each gain to set the sampling rate to 250 Samples/s. The output noise decreases from 1.5 LSB for gain of 1 to 1.1 LSB for gain of 16.

3.2 Neuropotential Interface Characterization

Figure 6a shows the measured frequency response of the front-end amplifier in the neuropotential interface channel. The amplifier bias was changed from 8 μ A to 100 nA resulting in a bandwidth change from 8.2 kHz to 140 Hz. The midband gain was measured to be 39.7 dB. The low cutoff frequency was smaller than 0.2 Hz implying that the high resistance elements were larger than 10^{12} Ω.

The amplifier's thermal noise level changed from 19 nV/$\sqrt{Hz}$ for 8.2 kHz bandwidth to 90 nV/$\sqrt{Hz}$ for 140 Hz bandwidth. This results in input-referred noise of 1.95 to 1.65 μV_{rms} for these bandwidth settings. The amplifier's NEF which is defined as[38]

$$\mathrm{N}EF = V_{n,rms}\sqrt{\frac{2I_{total}}{\pi \cdot U_T \cdot 4kT \cdot BW}} \tag{1}$$

was calculated to be below 3 for all bandwidth settings which compares favorably with NEF values between 3 and 10 reported in the literature. The amplifier also has CMRR (common-mode rejection ratio) and PSRR (power supply rejection ratio) of more than 70 dB and a total harmonic distortion (THD) of less than 1% for inputs less than 9.4 mV_{pp}.

The power spectrum of the digitized output when a 50 Hz 1 mV_{pp} sine wave is presented to the amplifier is shown in Fig. 6b. The amplifier bandwidth was set to 150 Hz. The ADC was set to 10 bit resolution and a gain of 1 leading to a sampling rate of 1 kS/s. THD of the channel was measured to be less than 0.3%. The channel noise in terms of LSB was 1.2 LSB (2.5 μV_{rms}) which is suitable for monitoring all modalities of neural potentials.
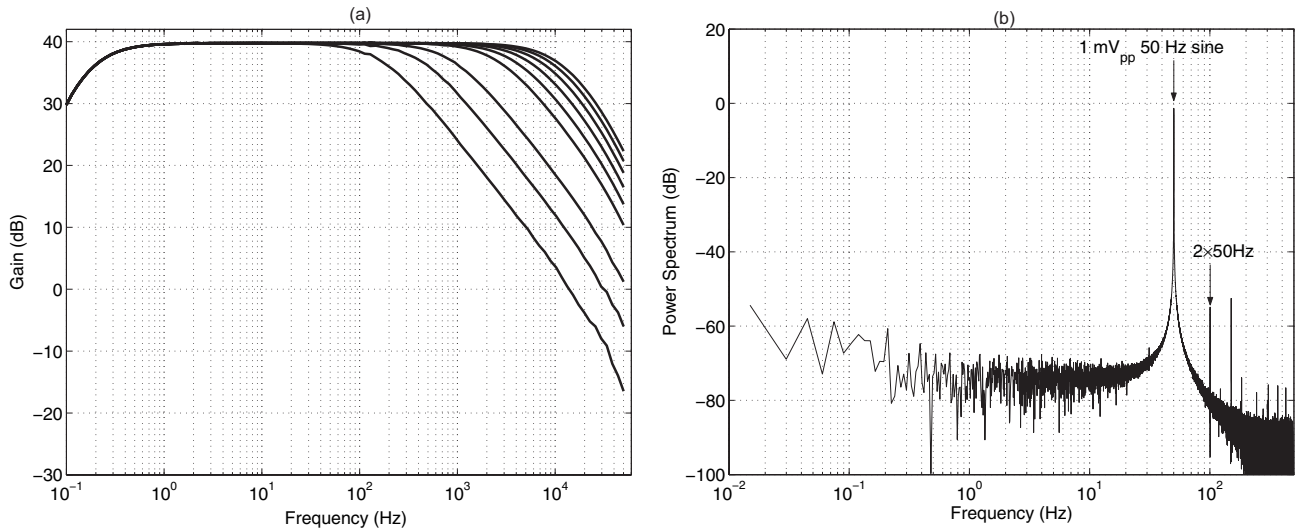

Figure 6. Neural interface characterization results. (a) Amplifier's frequency response for various bandwidths and (b) power spectrum of the recorded output when a 1 mV_{pp} 50 Hz sine wave is presented to the input.
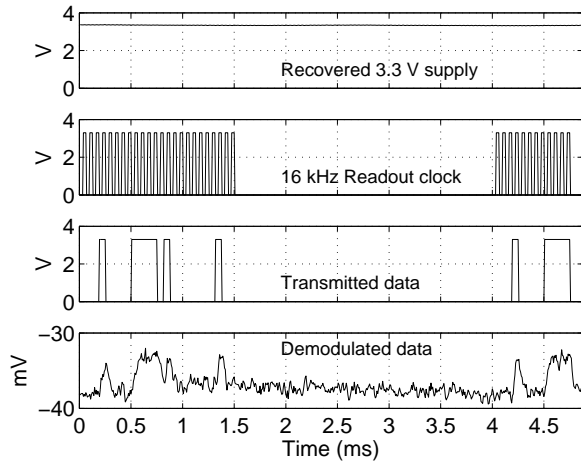
Figure 7. Test results from wireless operation showing the recovered 3.3 V power, readout clock generated from the recovered 1 MHz clock and transmitted & demodulated data.

Transmission rate 16 kbps			
Distance	Bits	Errors	BER
2 cm	480000	0	0
3 cm	480000	0	0
4 cm	480000	0	0
5 cm	480000	30	6.25×10^{-5}

Transmission rate 32 kbps			
Distance	Bits	Errors	BER
2 cm	480000	0	0
3 cm	480000	0	0
4 cm	480000	0	0
5 cm	480000	1630	3.39×10^{-3}

3.3 Wireless Operation

Figure 7 shows the regulated 3.3 V supply used to power the neuropotential/neurochemical chip. During the wireless operation of the system, the readout clock (second panel) is generated from the 1 MHz system clock provided by the telemetry module. With 24 pulses (left), both neurochemical and neuropotential interface data are read out while with 12 pulses (right), only the neuropotential interface data is shifted out. The plot also shows the digitized data from the two modules (third panel) as well as the demodulated data received on the base station (fourth panel). Table I shows the bit error rates measured up to 5 cm operation distance and 32 kbps operation distances. The module was able to provide stable supply power up to 5 cm during data transmission.
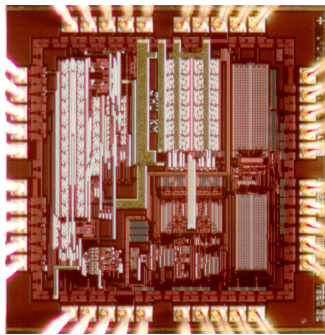
3.4 System Operation

Figure 8 shows micrographs of the neurochemical/neuropotential interface chip, the power harvesting & telemetry chip and acquired data from *in-vitro* wireless operation of the system. Prerecorded EEG data from rat somatosensory cortex were streamed from a function generator and a Kiethley 6430 sourcemeter was set to step
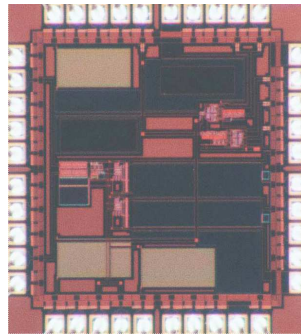

Neurochemical/neuropotential interface chip.
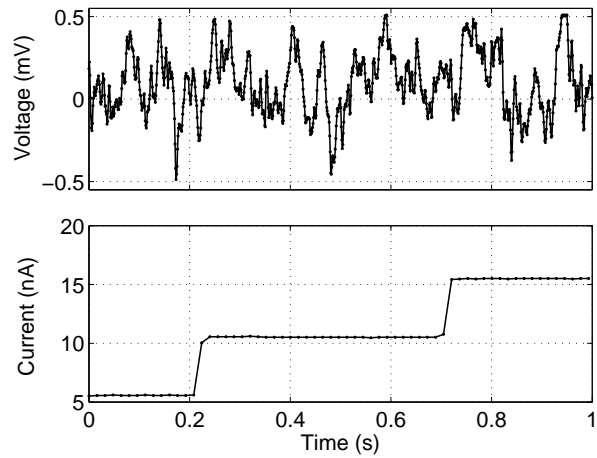
Power harversting and telemetry chip.

Figure 8. *Left:* Micrograph of the neurochemical/neuropotential interface. *Center:* Micrograph of the power harvesting/telemetry chip. *Right:* Demultiplexed data measured from the chip in an *in vitro* test. Top and bottom panels are prerecorded EEG data and current steps respectively.

the current to emulate neurochemical changes. The neuropotential interface was programmed with a digital gain of 1 and OSR of 2^{10} leading to a sampling rate of 1 kS/s. The neurochemical interface was set to a digital gain of 4 and an OSR of 2^{12} leading to a sampling rate of 64 S/s. The digital output of the chip was demultiplexed off-chip. The right panel of Fig. 8 shows the respective recovered eeg and current sweep waveforms.

4. CONCLUSION

We have presented a VLSI multimodal neural acquisition system for simultaneous wireless monitoring of neuropotential and neurochemical activity. The potentiostat module is able to monitor electroactive neurochemicals with picoampere sensitivity and offers configurable gain and resolution settings for wide range sensing. The channel consumes 42 μW of power from a 3.3 V supply. The neuropotential interface module offers tunable bandwidth from 140 Hz to 8.2 kHz and offers an input-referred noise of less than 2 μV_{rms} for all settings. The module also offers adaptive digital gain and ADC resolution settings for acquisition of neural potential of interest. The block consumes 100 μW of power at maximum bandwidth and sampling rate. The RF power harvesting and telemetry block was able to provide dual supplies and ADC clock for the system operation up to 4 cm and transmit data up to 32 kbps with BER less than 10^{-5}. The block consumed 35 μW of power itself.

Recent advances in VLSI biosystems offer a new tool to investigate the previously complicated studies in neuroscience. While most previous studies were purely electrical or used large and expensive instrumentation for neurochemical and neuropotential sensing, the presented integrated system opens a new avenue for real-time study of the interplay between neurochemical and electrical activity in awake behaving animals. We are planning to use this system to study the correlation between glutamate levels and EEG recovery in a cardiac arrest model in rats. Furthermore, the effect of hypothermia on these two signals and recovery following the ischemia will be studied.

REFERENCES

[1] Bear, M., Connors, B., and Paradiso, M., [*Neuroscience: Exploring the Brain*], Lippincott Williams & Wilkins (2006).

[2] Braman, R. and Hendrix, S., "Nanogram nitrite and nitrate determination in environmental and biological materials by vanadium (III) reduction with chemiluminescence detection," *Anal. Chem.* **61**, 2715–2718 (Dec 1989).

[3] Baranowska, I. and Zydron, M., "Liquid chromatography in the analysis of neurotransmitters and alkaloids," *J Chromatogr Sci* **40**, 224–228 (Apr 2002).

[4] Schlosser, R., "Detection of neurotransmitter interactions with PET and SPECT by pharmacological challenge paradigms," *Nervenarzt* **71**, 9–18 (Jan 2000).

[5] Malinski, T. and Taha, Z., "Nitric oxide release from a single cell measured in situ by a porphyrinic-based microsensor," *Nature* **358**, 676–678 (Aug 1992).

[6] Bard, A. and Faulkner, L., [*Electrochemical Methods: Fundamentals and Applications*], Wiley, New York (2001).

[7] Andersen, R. A., Musallam, S., and Pesaran, B., "Selecting the signals for a brain machine interface," *Curr. Opn. Neurobiol.* **14**(6), 720–726 (2004).

[8] Wolpaw, J. R., Birbaumer, N., McFarland, D. J., Pfurtscheller, G., and Vaughan, T. M., "Braincomputer interfaces for communication and control," *Clin. Neurophysiol.* **113**(6), 767–791 (2002).

[9] Hochberg, L. R., Serruya, M. D., Friehs, G. M., Mukand, J. A., Saleh, M., Caplan, A. H., Branner, A., Chen, D., Penn, R. D., and Donoghue, J. P., "Neuronal ensemble control of prosthetic devices by a human with tetraplegia," *Nature* **442**(13), 164–171 (2006).

[10] Murari, K., Stanacevic, M., Cauwenberghs, G., and Thakor, N., "Integrated potentiostat for neurotransmitter sensing. A high sensitivity, wide range VLSI design and chip," *IEEE Eng Med Biol Mag* **24**, 23–29 (2005).

[11] Turner, R., Harrison, D., and Baltes, H., "A cmos potentiostat for amperometric chemical sensors," *Solid-State Circuits, IEEE Journal of* **22**, 473–478 (Jun 1987).

[12] Kakerow, R., Kappert, H., Spiegel, E., and Manoli, Y., "Low-power single-chip cmos potentiostat," *Solid-State Sensors and Actuators, 1995 and Eurosensors IX.. Transducers '95. The 8th International Conference on* **1**, 142–145 (Jun 1995).

[13] Gore, A., Chakrabartty, S., Pal, S., and Alocilja, E. C., "A multichannel femtoampere-sensitivity potentiostat array for biosensing applications," *Circuits and Systems I: Fundamental Theory and Applications, IEEE Transactions on* **53**, 2357–2363 (Nov. 2006).

[14] Stanacevic, M., Murari, K., Rege, A., Cauwenberghs, G., and Thakor, N., "Vlsi potentiostat array with oversampling gain modulation for wide-range neurotransmitter sensing," *Biomedical Circuits and Systems, IEEE Transactions on* **1**, 63–72 (March 2007).

[15] Roham, M., Daberkow, D., Ramsson, E., Covey, D., Pakdeeronachit, S., Garris, P., and Mohseni, P., "A wireless ic for wide-range neurochemical monitoring using amperometry and fast-scan cyclic voltammetry," *Biomedical Circuits and Systems, IEEE Transactions on* **2**, 3–9 (March 2008).

[16] Webster, J. G., [*Medical Instrumentation, Application and Design*], Wiley and Sons, New York, NY, USA (1998).

[17] Dorman, M., Prisbe, M., and Meindl, J., "A monolithic signal processor for a neurophysiological telemetry system," *IEEE J. Solid-State Circuits* **20**(6), 1185–1193 (1985).

[18] Metting van Ring, A., Peper, A., and Grimbergen, C., "High-quality recording of bioelectric events," *Med. Biol. Eng. Comp.* **29**(5), 389–397 (1990).

[19] Ji, J. and Wise, K., "An implantable CMOS circuit interface for multiplexed microelectrode recording arrays," *IEEE J. Solid-State Circuits* **27**(3), 433–443 (1992).

[20] Martins, R., Selberherr, S., and Vaz, F., "A CMOS IC for portable EEG acquisition systems," *IEEE Trans. Instr. and Meas.* **47**(5), 1191–1196 (1998).

[21] Harrison, R. and Charles, C., "A low-power low-noise CMOS amplifier for neural recording applications," *IEEE J. Solid-State Circuits* **38**(6), 958–965 (2003).

[22] Mohseni, P. and Najafi, K., "A fully integrated neural recording amplifier with dc input stabilization," *IEEE Trans. Biomed. Eng.* **51**(5), 832–837 (2004).

[23] Patterson, W., Song, Y., Bull, C., Ozden, I., Deangellis, A., Lay, C., McKay, J., Nurmikko, A., Donoghue, J., and Connors, B., "A microelectrode/microelectronic hybrid device for brain implantable neuroprosthesis applications," *IEEE Trans. Biomed. Eng.* **51**(10), 1845–1853 (2004).

[24] Liu, W., Sivaprakasam, M., Wang, G., Zhou, M., Granacki, J., Lacoss, J., and Wills, J., "Implantable biomimetic microelectronic systems design," *IEEE Eng. Med. Biol. Mag.* **24**(5), 66–74 (2005).

[25] Sarpeshkar, R., Wattanapanitch, W., Rapoport, B., Arfin, S., Baker, M., Mandal, S., Fee, M., Musallam, S., and Andersen, R., "Low-power circuits for brain-machine interfaces," in [*IEEE Int. Symp. Circ. Sys. (ISCAS'2007)*], 2068–2071 (2007).

[26] Perelman, Y. and Ginosar, R., "An integrated system for multichannel neuronal recording with spike/LFP separation, integrated A/D conversion and threshold detection," *IEEE Trans. Biomed. Eng.* **54**(1), 130–137 (2007).

[27] Harrison, R. R., Watkins, P. T., Kier, R. J., Lovejoy, R. O., Black, D. J., Greger, B., and Solzbacher, F., "A low-power integrated circuit for a wireless 100-electrode neural recording system," *IEEE J. Solid-State Circuits* **42**(1), 123–133 (2007).

[28] Aziz, J., Genov, R., Derchansky, M., Bardakjian, B., and Carlen, P., "256-channel neural recording microsystem with on-chip 3D electrodes," in [*Tech. Dig., IEEE Int. Solid-State Circuits Conf. (ISSCC'2007)*], 160–594 (2007).

[29] Yazicioglu, R. F., Merken, P., Puers, R., and Van Hoof, C., "A 60 μW 60 nV/$\sqrt{\text{Hz}}$ readout front-end for portable biopotential acquisition systems," *IEEE J. Solid-State Circuits* **42**(5), 1100–1110 (2007).

[30] Denison, T., Consoer, K., Santa, W., Avestruz, A.-T., Cooley, J., and Kelly, A., "A 2 μW 100 nV/rtHz chopper-stabilized instrumentation amplifier for chronic measurement of neural field potentials," *IEEE J. Solid State Circuits* **42**(12), 2934–2945 (2007).

[31] Chae et al., M., "A 128-channel 6mW wireless neural recording ic with on-the-fly spike sorting and uwb tansmitter," *Solid-State Circuits Conference, 2008. ISSCC 2008. Digest of Technical Papers. IEEE International* , 146–603 (Feb. 2008).

[32] Vaillancourt, P., Djemouai, A., Harvey, J., and Sawan, M., "Em radiation behavior upon biological tissues in a radio-frequency power transfer link for a cortical visual implant," *Engineering in Medicine and Biology Society, 1997. Proceedings of the 19th Annual International Conference of the IEEE* **6**, 2499–2502 vol.6 (Oct-2 Nov 1997).

[33] Akin, T., Najafi, K., and Bradley, R., "A wireless implantable multichannel digital neural recording system for a micromachined sieve electrode," *Solid-State Circuits, IEEE Journal of* **33**, 109–118 (Jan 1998).

[34] Irazoqui-Pastor, P., Mody, I., and Judy, J., "In-vivo eeg recording using a wireless implantable neural transceiver," *Neural Engineering, 2003. Conference Proceedings. First International IEEE EMBS Conference on* , 622–625 (March 2003).

[35] Sauer, C., Stanacevic, M., Cauwenberghs, G., and Thakor, N., "Power harvesting and telemetry in CMOS for implanted devices," *IEEE Trans. Circuits Sys. I: Regular Papers* **52**(12), 2605–2613 (2005).

[36] Hille, B., [*Ionic channels of excitable membranes*], Sinauer Associates Sunderland, Mass (1992).

[37] Mollazadeh, M., Murari, K., Sauer, C., Stanacevic, M., Thakor, N., and Cauwenberghs, G., "Wireless integrated voltametric and amperometric biosensing," *Life Science Systems and Applications Workshop, 2006. IEEE/NLM* , 1–2 (July 2006).

[38] Steyaert, M. and Sansen, W., "A micropower low-noise monolithic instrumentation amplifier for medical purposes," *IEEE J. Solid-State Circuits* **22**(6), 1163–1168 (Dec 1987).